Carbon, 1975, Vol. 13, pp. 71–80. Pergamon Press. Printed in Great Britain

OXIDATION OF COMPRESSION ANNEALED PYROLYTIC GRAPHITES

G. S. RELLICK*, P. A. THROWER and P. L. WALKER, JR.

Department of Material Sciences, The Pennsylvania State University, University Park, Pennsylvania 16802, U.S.A.

(*Received* 26 *March* 1974)

Abstract—The reactivities of three highly crystalline, compression annealed pyrolytic graphites, designated APG142, G900, and G100 and differing in preferred orientation, crystallite size and defect content, were studied as a function of burn-off at 750°C and 20 Torr O_2 pressure. Large burn-off increments were achieved by oxidation at 900°C and about 30 Torr initial O_2 pressure. Measurements of bulk reaction anisotropy of the two principal surfaces (basal and edge) were found to correlate well with degree of preferred orientation and defect content. For two of the graphites, rate data taken on samples having wide variations in their basal surface to edge surface ratio could be normalized by expressing the rates in terms of an effective geometric edge area which takes into account the reaction anisotropy. However, the reactivity of APG142 samples, expressed in this same manner, was found to increase with increasing fraction of edge area, indicating a different mechanism for edge oxidation. Microscopic and macroscopic examination of oxidized specimens revealed a number of features including a high density ($\sim 10^5/cm^2$) of non-basal defects in the G100 material. A number of samples of APG142 and G900 showed a pronounced terracing effect at the layer plane edges. This is consistent with a mechanism of edge oxidation involving the migration of reactive species over the basal surfaces. A principal feature observed in all these materials was the occurrence of non-uniform oxidation at the edges, resulting in the formation of slit shaped voids running parallel to the layer plane direction. The possible role of lattice vacancies, non-basal dislocations and grain boundaries in the overall oxidation process has been examined by developing idealized models involving preferential attack at these defect sites.

1. INTRODUCTION

Many of the discrepancies in reported values for kinetic parameters of the carbon–oxygen reaction can be traced to marked differences in structure of the various carbon materials used. It is now generally agreed that graphite oxidation occurs principally at peripheral edge carbon atoms which are exposed not only at prismatic surfaces but also at lattice discontinuities such as vacancies, non-basal dislocations and inter-crystallite boundaries. The number of edge sites and the extent to which further sites are developed with burn-off will depend on the nature and magnitude of these defect parameters. Because highly oriented pyrolytic graphites, produced by the thermal annealing or compression annealing of pyrolytic carbons, are amenable to structural characterization, they offer an excellent opportunity for examining the influence of various structural features on reactivity.

While a good deal of work has been done examining the structure and measuring physical properties of these materials, little attention has been paid to their reactivity in oxidizing gases. The results reported here serve to provide further characterization of highly oriented pyrolytic graphites, since relations between their structure and reactivity have been found.

*Present address: ICI America Inc., Marshall, Texas.

†Geometric areas are calculated, by definition, assuming roughness factors equal to one.

2. EXPERIMENTAL

2.1 *Materials*

The pyrolytic graphites used in this study were supplied by the Carbon Products Division of Union Carbide Corporation. They were reportedly deposited from methane at about 2200°C and subsequently annealed under pressure at temperatures greater than 3000°C. The specimens were designated as APG142, G900 and G100. In physical appearance, APG142 differed from the other specimens in that it still retained the growth cone structure, characteristic of as-deposited pyrolytic graphites. Samples of G900 and G100 had no visible growth features.

Individual samples were cut into parallelpiped sections of variable size from the original specimen blocks by means of a high speed slitting saw. After cutting, the samples were cleaved to the desired thickness by repeated application of cellophane tape. This also permitted removal of the original contaminated basal surfaces. A summary of the ratios of geometric basal to geometric edge areas prepared for the different samples is given in Table 1†. A total of six, four and three samples of

Table 1. Geometric basal area to geometric edge area ratios (A_b/A_e) for samples used in this study

APG142	G900	G100
4 (2)*	2 (2)	9
6	4	10
11	7	60
12 (2)		

*Indicates number of samples.

APG142, G900 and G100, respectively, were used in this study.

In order to reduce the roughness introduced in the cutting, the edges of the samples were polished with progressively finer grades of abrasive paper. Care was taken to minimize the extent of shear deformation resulting from this process. It has recently been shown that deformation of structure at the edges of annealed pyrolytic graphites results in high initial carbon gasification rates [1]. Since the cutting and handling involved in the preparative procedures served as likely sources of undesirable contamination, it was deemed necessary to heat-treat the samples to eliminate possible catalytic effects. Heat-treatment was carried out in a graphite resistance tube furnace. Samples were slowly heated in an atmosphere of flowing argon to a maximum temperature of 2500°C. They were held at this temperature for about 20 min before being cooled slowly to room temperature. The oxygen used was J. T. Baker Company ultra pure grade.

2.2 *Apparatus*

In the course of a reactivity run, the carbon weight loss was monitored by a Cahn RG Electrobalance connected to a multi-speed Honeywell recorder. The graphite samples were held in a quartz cradle and suspended from the balance by means of a quartz fiber. The static reactor system (4 l. volume) was evacuated using a two-stage mercury diffusion pump and a Vac-Ion gettering pump. The samples were enclosed within a double-walled hangdown tube and were heated by means of a resistance furnace, the temperature of which was controlled by a Leeds and Northrup controller. Temperature control was maintained to within ±2°C at 750°C. More accurate temperature measurements were made with a chromel–alumel thermocouple connected to a Leeds and Northrup potentiometer.

Measurements of c-axis orientation of the pyrolytic graphites were made using a Siemens Pole Figure Diffractometer in conjunction with a Picker Proportional Counter. The counter automatically records the variation of diffracted intensity as a function of angle ϕ, defined as a positive or negative rotation away from the Bragg angle where, by definition, $\phi = 0°$. From these data, the mosaic spread, defined as the angular width at half-maximum intensity is determined.

Determination of the crystallite size, L_a, was made by examining optical micrographs of the basal surfaces of samples that had been etched for about 20 min at 750°C and 20 Torr O_2 pressure.

2.3 *Procedure*

Since the cutting and polishing procedures introduced variable degrees of edge roughness, all samples were subjected to an initial burn-off of about 10 per cent at 900°C before the first reactivity run was made. Prior to a reactivity run, the sample was outgassed at 950°C using a Vac-Ion pump for 6 hr to remove possible adsorbed surface oxide. Reactivity runs for the pyrolytic graphites were made at 750°C and 20 Torr O_2 pressure. Total burn-off during each reactivity run was usually 0·2 per cent. Large burn-off increments were achieved, between reactivity runs, by reacting the specimens at 900°C and about 30 Torr initial O_2 pressure. Following each large incremental burn-off, the sample was removed from the reactor and its geometric dimensions measured. The sample thickness, which corresponded predominantly to the c-axis direction, was measured to the nearest 0·001 mm with a micrometer. Because of the fragile nature of the sample edges, the basal plane dimensions were measured using a centimeter rule. These measurements were accurate to ±0·2 mm.

3. RESULTS AND DISCUSSION

3.1 *Structural characterization*

Figures 1a and 1b show the etched surfaces of APG142 and G900. The magnitude of L_a is ~50 μm for G900 and ~20 μm for APG142. The etched surfaces of G100 (Fig. 1c) reveal a relatively high density (~10^5/cm^2) of non-basal defects but no clearly recognizable crystallites. A number of the defects are seen to completely penetrate the sample thickness.

Table 2 summarizes the mosaic spread values for the three different pyrolytic graphites. Measurements made with the X-ray beam incident on the two basal surfaces showed, for APG142 and G100, that one side was slightly more oriented than the other. For samples of APG142, which still retained some semblance of the original growth cone structure, the less oriented side was identified as that nearest the original substrate surface [2].

3.2 *Measurements of reaction anisotropy*

The determination of the effective anisotropy for reaction occurring in the directions parallel and perpendicular to the layer planes ($R_{a/c}$) was made by following

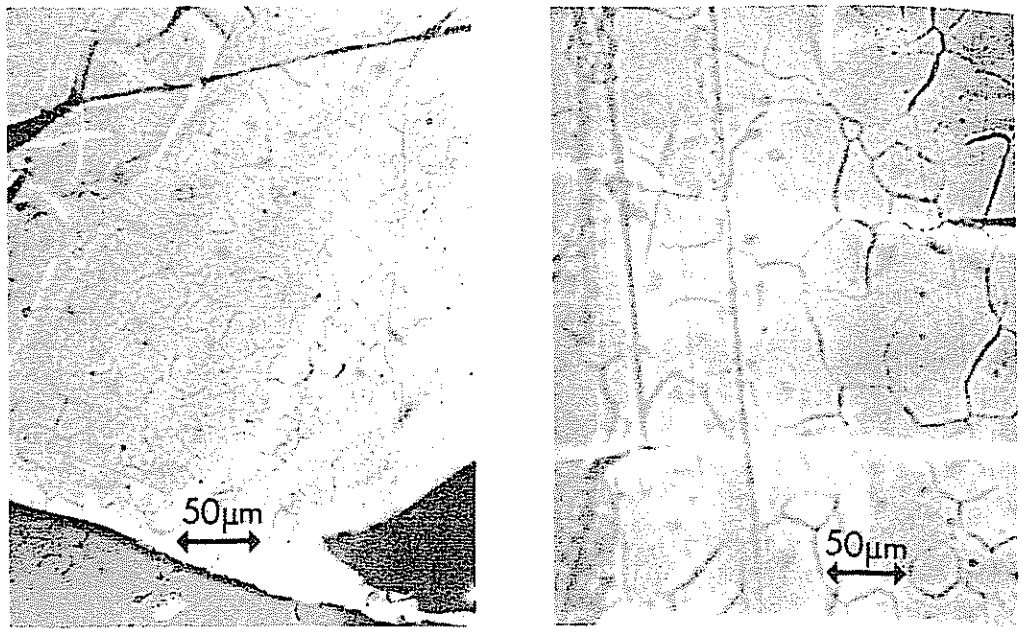

(a) (b)

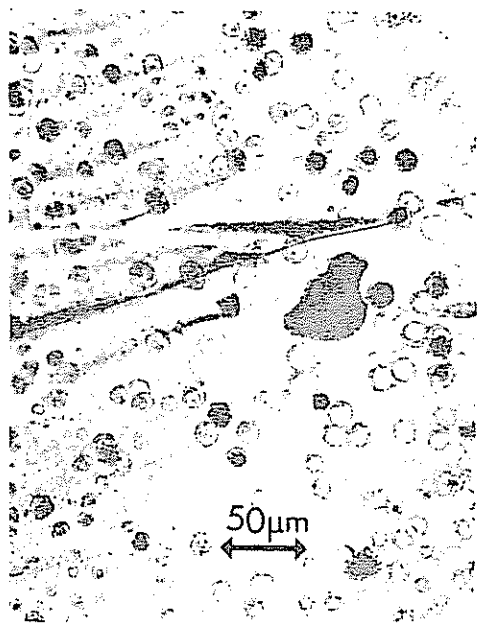

(c)

Fig. 1. Optical micrographs of etch surfaces of (a) APG142, (b) G900, and (c) G100.

Table 2. Mosaic spread values for different pyrolytic graphites

Sample	Mosaic spread (Degrees) Side 1	Side 2
APG142	4·4	3·1
G900	1·4	1·4
G100	5·4	4·8

decreases in sample dimensions with oxidation. Typical plots of Δc (decrease in thickness) vs Δa (decrease in basal plane length) for the different materials are shown in Fig. 2. The last data points for samples APG142, G900 and G100 correspond to cumulative burn-offs of 77 per cent, 80 per cent, and 78 per cent, respectively. Results for all the samples are summarized in Table 3. Since the bulk reaction anisotropy is expected to be primarily dependent upon the relative crystallite alignment, these results are to be compared with measurements of preferred orientation given in Table 2. Good qualitative agreement is found between low mosaic spread values and high reaction anisotropy. However, the large difference between values of $R_{a/c}$ for the APG142 and G100 materials may not be explained solely by differences in their crystallite alignment. The markedly lower value of reaction anisot-

Table 3. Reaction anisotropy ratios for different pyrolytic graphites

Sample	$R_{a/c}$
APG142	24 ± 2 (6)*
G900	30 ± 2 (3)
G100	14 ± 2 (3)

*Numbers in parentheses indicate samples used to obtain averages.

ropy for G100 could also be attributable, in part, to the large concentration of non-basal defects in this material.

3.3 *Reactivity data*

One of the principal objectives of the reactivity studies was to determine a method for expressing the specific reactivity for samples of different sizes and shapes, that is rate per unit surface area. In an earlier study of the reaction of oxygen with a stress-recrystallized pyrolytic graphite, Baker[3] found that reactivities could be normalized if they were simply expressed in terms of the geometric edge area, neglecting the contribution of the basal plane area to reactivity. Obviously, the extent to which this approach leads to a good approximation of over-all reactivity depends upon the reaction anisotropy of the materials and their basal to edge area ratio. For samples having a relatively low reaction anisotropy and/or a high basal to edge area ratio, it is necessary to express specific rates in terms of the relative contributions of the two principal surfaces to reactivity. A first approach is to express the rate in terms of an effective geometric edge area given by

$$A_{\text{eff}} = A_e + \beta A_b,$$

where A_e and A_b are the geometric edge and basal areas, and β is a weighting factor equal to the anisotropy ratio, $R_{c/a}$ (that is $1/R_{a/c}$).

For the APG142 samples the largest value of A_b/A_e was about 12, and the results expressed in terms of edge area were not too different from those expressed in terms of A_{eff}. However, for one G100 sample the A_b/A_e ratio was about 60. In this case it was found that the rate could only be normalized by using the A_{eff} term. Reactivities per unit A_{eff} for the graphites are shown in Figs. 3 and 4. There is no significant effect of the A_b/A_e ratio on reactivities expressed per unit A_{eff} for samples G900 and G100, as seen in Fig. 3. That is, specific rates for different shaped samples were essentially the same at comparable degrees of burn-off. For G900, rates were independent of burn-off after about 35 per cent burn-off, while for G100,

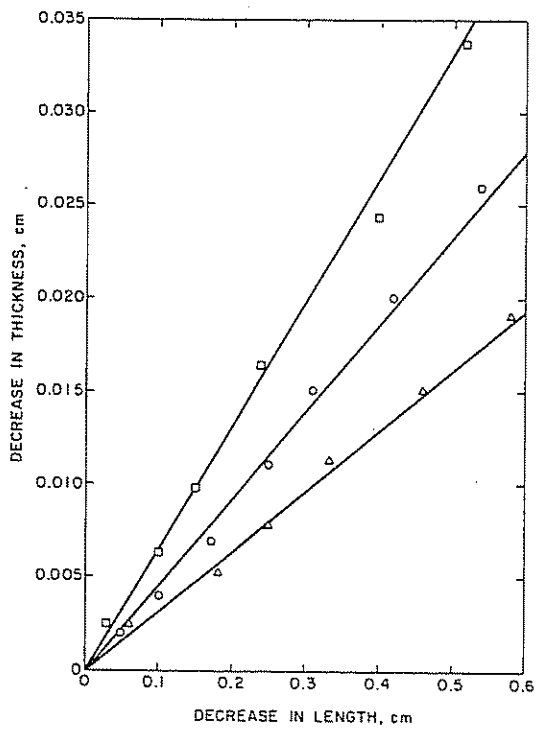

Fig. 2. Decrease in thickness vs decrease in length for samples upon oxidation. □ G100, ○ APG 142, △ 900.

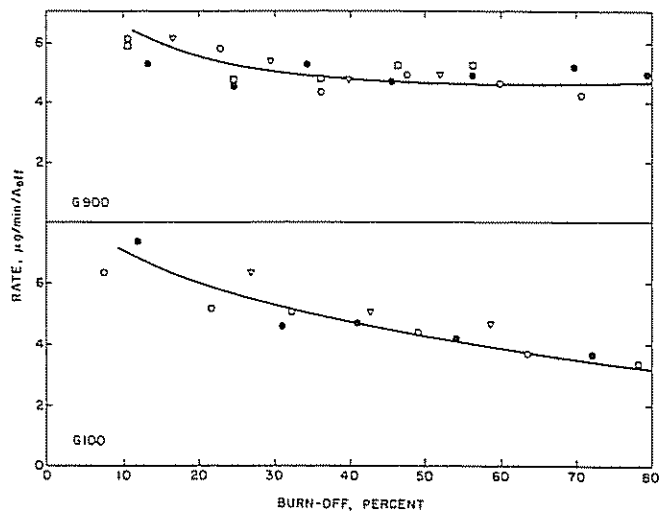

Fig. 3. Change of specific rate of oxidation with burn-off for samples of G900 and G100 of various A_b/A_e ratios.

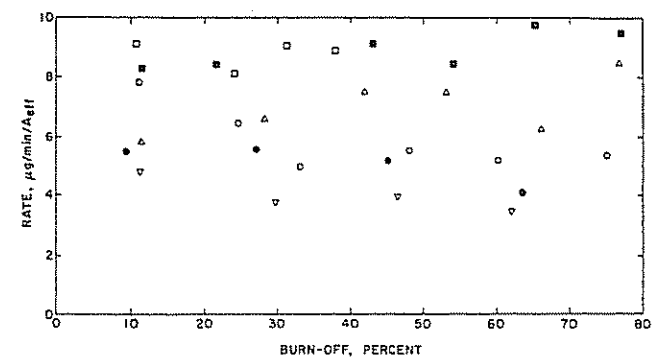

Fig. 4. Changes of specific rate of oxidation with burn-off for samples of APG142 of various A_b/A_e ratios: □ ▣ 4, △ 6, ○ ◉ ▽ 11·5.

rates decreased steadily with increasing burn-off. As seen in Fig. 4, reactivities for APG142 could not be normalized for sample shape by dividing by A_{eff}.

At first it was thought that the scatter could be explained by the slight difference in orientation between the two basal surfaces. That is, Horton and Ballard[4] have recently reported that one of the major features of the oxidation of a thick specimen of as-deposited pyrolytic graphite is the non-uniformity of edge attack as a function of distance from the substrate surface. They also found that the substrate surface was more extensively oxidized than the top basal surface and that the diameter of holes produced in the substrate surface following oxidation was an order of magnitude larger than those generated at the top basal surface. With this in mind, reactivity runs were made on one sample of APG142 cut from the top of the block (where deposition last occurred) and another sample cut from the bottom (substrate) side of the block. Both samples had the same dimensions. Plots of rate vs per cent burn-off were essentially the same for both samples, however, indicating that the scatter in reactivity results could not be attributed to differences in distance of deposition of the sample from the original substrate. A closer examination of the reactivity data revealed that the specific rates could be grouped into three regions or bands according to their basal to edge area ratios. It is seen from Fig. 4 that samples with higher fractions of edge area have higher specific reactivities in almost every case. Of the thirty data points plotted, only three failed to fall into this general pattern. Since the basal areas of all the samples were nearly the same, differences in the ratios A_b/A_e are due primarily to variations in sample thickness. These results are consistent with those of Evans *et al.*[5] who found that at 840°C, multilayer steps on graphite single crystals receded at a much higher rate than did monolayer steps.

The idea of using a geometric area to correlate reactivity results should not be taken to imply that we feel negligible surface roughness exists in the samples, particularly after substantial oxidation has occurred. Fig. 5 is a scanning electron micrograph of an edge of an APG142 sample oxidized to 77 per cent burn-off. It is clear that delamination has occurred along the layer plane directions, exposing additional basal area at the sample edges. A rough measure of the magnitude of the internal volume (roughness) resulting from this delamination can be obtained by plotting the percentage change in geometric volume vs per cent burn-off for each sample. This is shown in Fig. 6. There is no significant difference in the magnitude of internal burning for the three materials. The averaged slope of the experimental curve is approximately 0·9 compared to 1·0 for the ideal curve with no development of internal volume. This

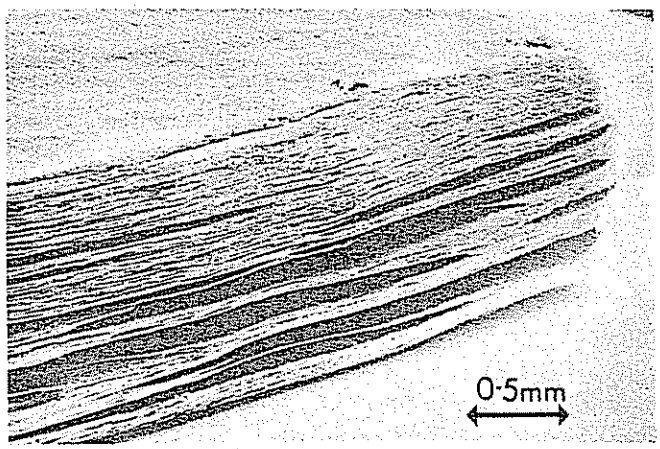

Fig. 5. Scanning electron micrograph of the edge surface of APG142 oxidized to 77 per cent burn-off.

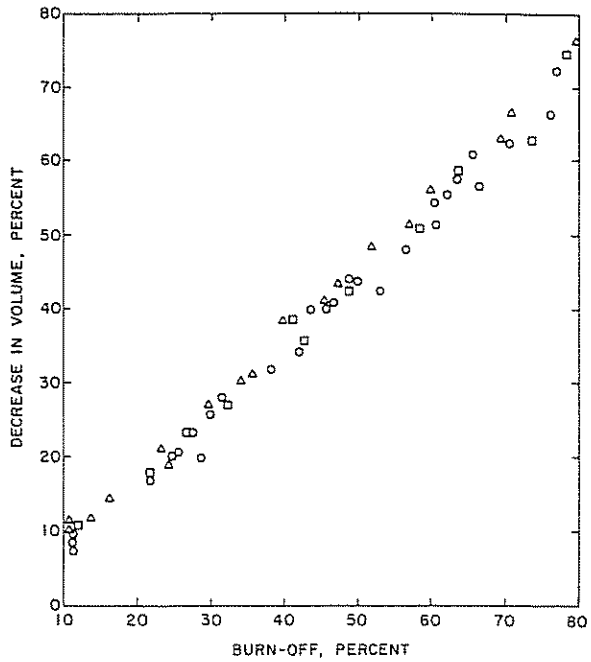

Fig. 6. Decrease in external volume of graphite samples with burn-off. Data from all runs are included.

indicates that the burn-off can be closely approximated by a contracting parallelpiped model.

Results such as those shown in Fig. 6 do not provide a direct estimate of the basal area exposed at the edge of samples since this depends on the size and number of voids produced. If the void volume consists of a small number of large voids, the basal area produced will be relatively small. On the other hand, if edge oxidation produces numerous small voids, the basal area resulting can be quite significant. Hennig[6] has argued that the maximum steady-state roughness factor for the geometric edges of single crystals would be equal to $R_{a/c}$ and that this condition would prevail only if the initial roughness were greater than or equal to $R_{a/c}$.

This model does not, however, take into consideration

the kind of preferential edge oxidation that is seen to occur with the samples used in this study. Examination of the edges of oxidized samples reveals, as in Fig. 5, a number of large voids suggesting that the additional basal area produced is minimal. A more convincing arguement is provided by the data on two samples of G100, which had the same basal plane areas, but differed in thickness by a factor of six. The thicker sample was found to be approximately twice as reactive as the thinner one at comparable degrees of burn-off. The edge roughness factor, R, needed to produce a two-fold rate increase for a six-fold edge area increase can be calculated from the expression

$$6(A_e + R\beta A_e) + \beta A_b = 2(A_e + R\beta A_e + \beta A_b)$$

where A_e and A_b are the geometric and basal areas for the thinner sample, and β is the anisotropy ratio, $R_{c/a}$, which for G100 samples was found to be equal to 1/14. The value of A_b/A_e was about 60; R under these conditions is calculated to be about 1·4. That is to say that the basal area accessible *via* the sample edges, resulting from gasification, is 40 per cent of the geometric edge area. Unfortunately, it was not possible to obtain other samples with the same range of thickness. Our conclusions regarding edge roughness are, therefore, only preliminary at this time.

3.4 *Topographical features of oxidized samples*

In addition to the preferential attack occurring at the sample edges, a number of other interesting macroscopic and microscopic features were noted. A major feature of unoxidized samples of APG142 was the presence of convex and concave asperites on the top and bottom basal surfaces respectively. If the primary mode of basal plane oxidation involved attack along the cone axes, the surface convexities would be expected, after some period of oxidation, to be effectively converted into corresponding surface depressions. This, in fact, was not found to be the case. Rather, it was found that basal plane attack was quite uniform and that the top and bottom surfaces could usually be distinguished up to about 60 per cent burn-off. In one case, the concave and convex surfaces remained clearly distinguishable after 82 per cent burn-off. Figure 7 shows a typical surface of an APG142 sample oxidized to 77 per cent burn-off. The uniformity of layer plane removal and the similarity between values of $R_{a/c}$ for APG142 and G900 suggest that, for APG142, the growth cones were not important in determining the characteristics of basal plane oxidation.

A particularly interesting, though not unique, feature of APG142 oxidation is shown in Fig. 8. The layer planes are seen to be terraced as a result of faster edge oxidation of the planes nearest the top surface. Terracing was even more pronounced in a G900 sample shown in Fig. 9. This same effect has been observed at a microscopic level by other workers. Adamson *et al.*[7], using radiolytic CO_2, observed that thin areas of single crystal surfaces were oxidized more rapidly than thicker areas and that stepped

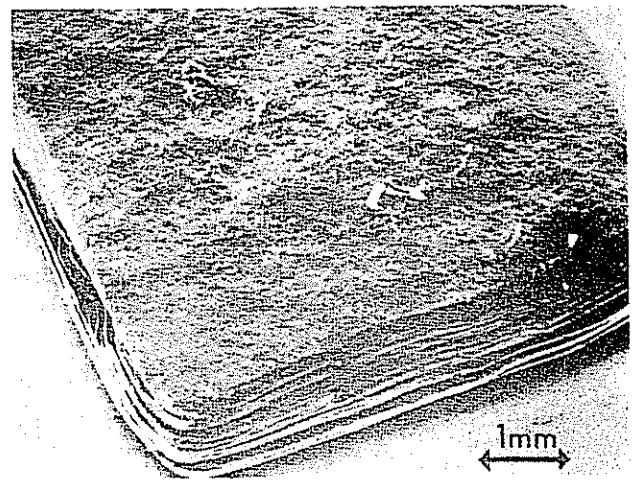

Fig. 7. Scanning electron micrograph of the basal plane surface of APG142 oxidized to 77 per cent burn-off.

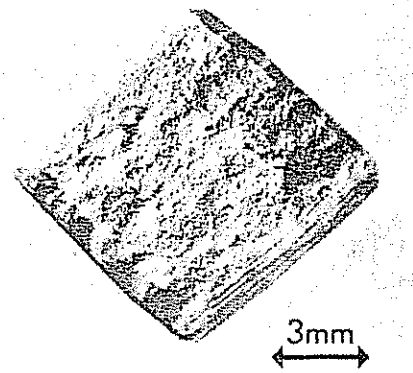

Fig. 8. Optical micrograph of APG142 oxidized to 60 per cent burn-off showing terraced edges.

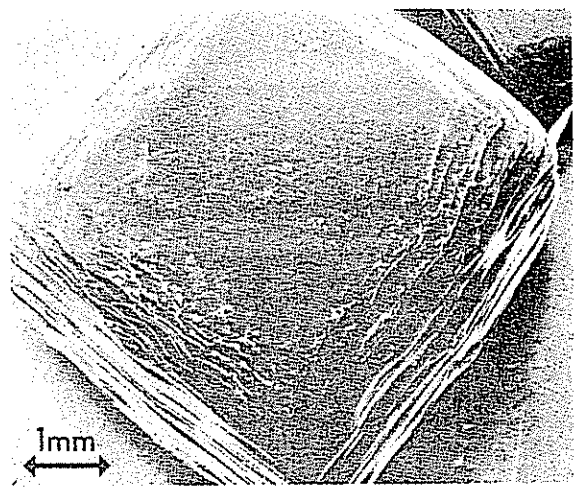

Fig. 9. Scanning electron micrograph of G900 oxidized to 57 per cent burn-off showing terraced edges.

edges were attacked more rapidly than cliff edges. Similarly, Feates[8] and Feates and Robinson[9] found that only the uppermost layer of a multilayered edge face recedes; and only after the top layer exposes basal area of the next lower lying plane, does that plane begin to recede. These authors have interpreted this as being consistent with a mechanism involving adsorption of active species on the basal plane which migrate over the surface until they find reactive sites, such as defects or step edges. Under these conditions the rate of edge recession would be proportional to the basal "collector area" if the rate of direct abstraction from the basal planes was low. Furthermore, the probability of reactant species diffusing across the layer plane surfaces and reaching the specimen edges would depend on the relative concentrations of reactive edge sites on the basal surfaces. A reasonable indicator of this would be the ratio $R_{a/c}$. This argument is supported by the fact that terracing was not found to occur in any of the samples of G100, which had the lowest value of $R_{a/c}$.

Conclusions drawn here are only tentative since marked terracing was found to a pronounced degree in only a few of the samples. In fact, the opposite side of the sample in Fig. 9 showed a uniformly eroded edge. A closer examination of Figs. 8 and 9 reveals that the terracing effect of these samples is actually confined to a relatively small number of layer plane packets which tend to recede as a unit. This was somewhat more noticeable in the G900 sample. We suspect that this may be related to a larger structural macro-unit such as that observed by Rodriguez-Reinoso and Thrower[10] in a similar stress-recrystallized pyrolytic graphite.

As shown earlier in Fig. 1c, oxidized samples of G100 were characterized by a predominance of non-basal defects having a density of $\sim 10^5/cm^2$. Figure 10 is a G100 sample after a 20 min etch showing two screw dislocations connected by a common cleavage step. A number of partially reacted defect sites are revealed in Fig. 11. It can be seen that attack is initiated at the center or core of the defect and then proceeds outward. Figure 12 shown the surface of a G100 sample oxidized to about 20 per cent burn-off. An interesting mosaic is produced by the coalescence of etch pits. The density of pits is also $10^5/cm^2$, indicating that they are the same defects shown in the preceding figure. Figures 13a and 13b show opposite surfaces of a very thin G100 sample oxidized to 74 per cent burn-off. A number of much larger defects is seen to occur predominantly on one side. The thickness of the sample was 75 μm, giving an upper limit for the depth of the defects.

3.5 *Defect models for basal plane reactivity*

The anisotropy ratio for reactions occurring at edge planes and defectfree regions of the basal planes has been estimated by Hennig[11] to be about 10^{13}. On the other hand, measurements of the depths and radii of etch pits within basal planes indicate that the ratio of the rate of advance in the a-direction to that in the c-direction is

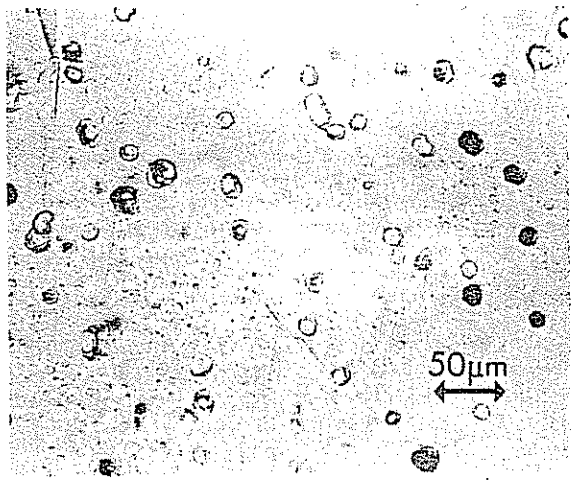

Fig. 10. Etched surface of G100 showing two screw dislocations.

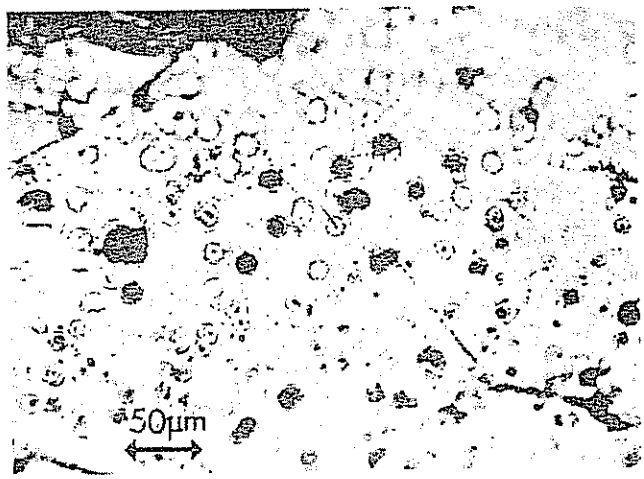

Fig. 11. Etched surface of G100 revealing preferential attack at defect cores.

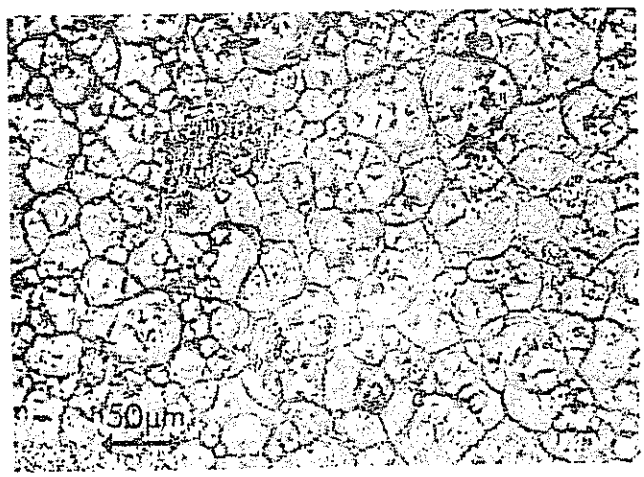

Fig. 12. Mosaic character of basal surface of G100 following oxidation to 20 per cent burn-off.

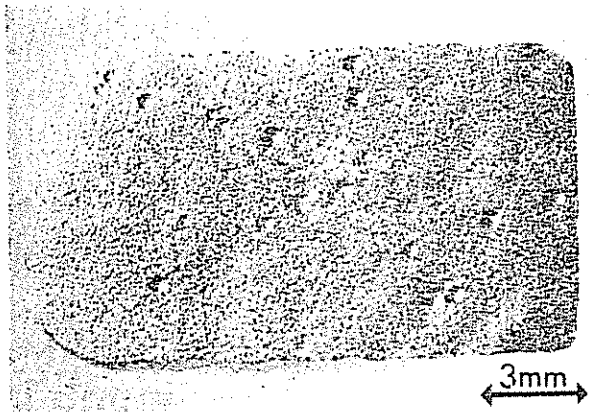

(a)

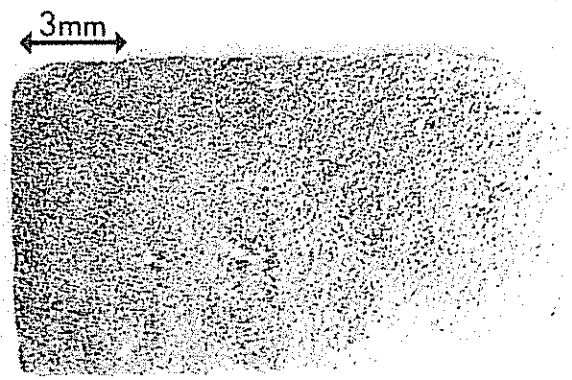

(b)

Fig. 13. Opposite basal plane surfaces of a 75 μm thick G100 sample oxidized to 74 per cent burn-off. Note concentration of large non-basal defects on the surface in (a).

reduced to about 25 at defect sites not deliberately contaminated with impurities [12]. The similarity between this value and the bulk values of $R_{a/c}$ obtained in this study, along with Hennig's results, suggests that the effective c-axis oxidation rate is closely associated with the nature and magnitude of defects within the basal planes. Some possible relationships have been examined by constructing a number of idealized models which attempt to relate the overall rate of layer plane removal to the local reactions occurring at various defect sites.

For the case of single lattice vacancies, the model is based on the following assumptions:

(1) The vacancy density, given by n/cm^2, is the same for all layer planes in the lattice.

(2) The vacancies are uniformly distributed over the surface such that a $1\,\text{cm}^2$ area of basal area has $\sqrt{n}$ vacancies along an edge.

(3) The rate constant for radial expansion, k, expressed in cm/sec, is the same as that for specimen edges.

(4) The value of k is independent of loop diameter.

(5) Coalescence of all vacancies occurs simultaneously. At this point the layer plane is completely removed and the radius of the expanded vacancy is given by $1/2\sqrt{n}$. (Actually, only about 80 per cent of the surface would be removed, but for the degree of accuracy sought, the assumption is quite satisfactory.)

(6) The formation rate of new vacancies is negligibly small.

The radius of a vacancy at time t is given by

$$r(t) = r_0 + kt,$$

where r_0 is the original radius of the unexpanded vacancy ($\sim 2A$). The first layer plane will be removed when $r(t) = 1/2\sqrt{n}$. The time required for this is

$$t_b = \frac{\frac{1}{2\sqrt{n}} - r_0}{k},$$

which for reasonable values of n, simplifies to

$$t_b \cong \frac{1}{2k\sqrt{n}}.$$

Using a thickness of $3{\cdot}35 \times 10^{-8}$ cm per layer plane, the effective rate in the c-axis direction is given by

$$R(\text{basal planes}) = 7{\cdot}7 \times 10^{-8}\, k\sqrt{n}, \frac{\text{cm}}{\text{sec}}.$$

The anisotropy ratio, $R_{a/c}$, is, therefore,

$$R_{a/c} = \frac{1}{7{\cdot}7 \times 10^{-8}\sqrt{n}}$$

For $R_{a/c} = 25$, $n \approx 3 \times 10^{11}$ vacancies/cm^2. This applies only to the top layer plane, however; and it is clear that as vacancies in this plane are expanded, progressive oxidation of the next layer plane will occur as existing vacancies are revealed. An estimate of the extent to which the second layer plane is oxidized at the point which the first layer plane has been removed (at $t_b = 1/2\sqrt{n}$) can be obtained by noting that the area of an expanded vacancy in the first plane at time t is given by

$$A_1(t) = \pi(r_0 + kt)^2.$$

The total area of the second layer plane exposed is

$$A_2(t) = n\pi(r_0 + kt)^2,$$

for one square centimeter of basal area. The number of vacancies revealed withing this area is calculated from

$$N_2(t) = n^2\pi(r_0 + kt)^2.$$

It is necessary then to know the number of vacancies which have been exposed for increments of time ranging from $t = 0$ to $t = t_b$. This suggests defining a dimensionless variable, τ (or characteristic time), such that

$$\tau = \frac{t_b - t}{t_b},$$

and expressing the number of vacancies exposed in the second layer plane as a function of τ. The fraction of the second plane removed then is given by

$$f_2 = \frac{\int_{\tau=1}^{\tau=0} N_2(\tau)\,\mathrm{d}\tau}{n}$$

Evaluating the integral gives

$$f_2 = \frac{n\pi}{3}(kt_b)^2$$

Recalling that $kt_b = 1/2\sqrt{n}$ gives

$$f_2 = 0{\cdot}26,$$

and f_2 is seen to be independent of n.

Since only about 25 per cent of the second layer plane is removed, deeper planes are even less significantly oxidized, and steady-state gasification is confined to only the top few layer planes. The effective rate of layer plane attack is, therefore, increased only slightly and the required vacancy density is still on the order of $10^{11}/\mathrm{cm}^2$. The value of k for vacancy expansion has been assumed here to be the same as for edge recession. The recent work of Evans *et al.*[5] indicates that this figure may in fact be smaller than for multilayer edges. Consequently, this assumption tends to produce a value of n which is low. The assumption that the expanded vacancies coalesce simultaneously also leads to a low value for n. The maximum vacancy density which could be quenched into the lattice from 3000°C is about $10^6/\mathrm{cm}^2$[13]. It is, therefore, concluded that the rate of layer plane removal cannot be accounted for primarily by the existence of vacancies.

A similar type of model can be developed by postulating that basal plane reaction is initiated at crystallite boundaries followed by edge attack of individual crystallites. This is shown schematically in Fig. 14. As attack proceeds down the grain boundary at a rate k_g, the crystallite edges recede at a rate given by k. After the topmost layer plane has been completely removed, steady-state gasification commences; and individual layer planes are removed at the same rate as new layer planes are being exposed. This, of course, is simply k_g.

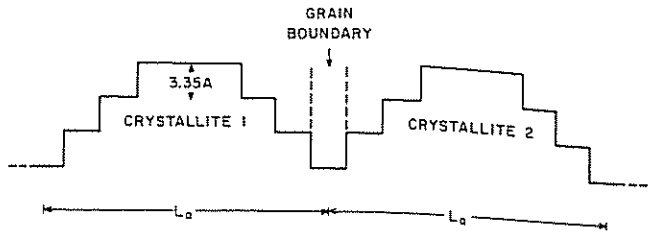

Fig. 14. Diagram of model involving preferential oxidation at grain boundaries followed by edge attack of individual crystallites.

Therefore, after the onset of steady-state gasification of the basal surfaces, the value of $R_{a/c}$ is given by k/k_g. Unfortunately, no reliable value for this ratio is known. Furthermore, it would be expected to vary with the relative misorientation of crystallites. The effective c-axis rate would also be less than k_g due to the boundary encountering a crystallite surface after being oxidized a distance L_c. At this point it could be argued that the crystallite must then recede laterally an average distance of $L_a/2$ before encountering a new boundary, assuming a uniform distribution of crystallites. That is, the effective rate is determined by the time required to oxidize a distance $L_c + L_a/2$ at rates of k_g and k, respectively. This leads to an approximate expression for the effective rate,

$$k_g' = \frac{2kk_g}{2k + nk_g},$$

where $n = L_a/L_c$. Since values of L_a are generally much larger than L_c for highly oriented pyrolytic graphites[10, 14], the effective c-axis rate, k_g', would be significantly diminished below the value of k_g. For example, if $L_a/L_c \simeq 200$[10] and $k/k_g = 25$, then $k_g' = 0{\cdot}2\,k_g$. The effective anisotropy ratio, $R_{a/c}$, would be about 125, which is not in agreement with experimentally measured values. However, if $L_a/L_c = 10$, and $k/k_g = 25$, then $k_g' \cong k_g$.

A similar type of model can be postulated based on preferential oxidation down the cores of non-basal dislocations[15]. Thomas and Roscoe[16] have shown that such dislocations frequently traverse a number of inter-crystallite boundaries. In this case, the rate of layer plane removal would not be as affected by the ratio L_a/L_c; and oxidation would proceed at a rate close to k_d (c-axis rate at the dislocation core).

3.6 *Estimates of edge area at defect sites*

Estimates of the edge area produced in the basal planes by the preferential oxidation of various defects can be made. For the case of fully expanded vacancies, the final pit diameter is given by $1/\sqrt{n}$. The circumference of the pit is then $\pi/\sqrt{n}$. Around the circumference of the

expanded vacancy, the linear density of carbon atoms is about 1 atom per 2·5A. The number of edge atoms per vacancy is given by $10^8/\sqrt{n}$, and the number of exposed edge atoms in one square centimeter of basal area is $\sqrt{n}10^8$. For $n = 10^8/cm^2$, the number of edge atoms is $\sim 10^{12}$ per cm^2 of basal surface. For 1 cm^2 of edge area there are $\sim 10^{15}$ atoms, taking $8{\cdot}3A^2$ as the area of an edge plane atom. Therefore, for equal units of basal and edge area, the reactive sites in the basal plane would contribute only 0·1 per cent of the total number of such sites. This value is increased slightly by allowing for exposed vacancies in lower lying planes. For most samples, the basal area is larger than the edge area and the overall contribution of the vacancies is increased by the factor A_b/A_e. For specimens such as those used in this study, where A_b/A_e was frequently larger than 10, the vacancies would be expected to contribute about 1 per cent of the total sample reactivity if $n = 10^8/cm^2$. For an edge roughness factor of 25, the vacancies in the basal planes would still only contribute about 3·5 per cent to the reactivity.

The maximum edge area exposed upon gasification at crystallite boundaries can be evaluated from the idealized model shown in Fig. 14. It can be shown[15] that the amount of edge area produced per unit geometric basal plane area in this case is exactly equal to the anisotropy ratio, k_g/k and is independent of crystallite diameter. If we take $k_g/k = 1/25$ and $A_b/A_e = 10$, the basal planes will contribute about 30 per cent to the sample reactivity through their exposed edge surface. Obviously the contribution of reaction at basal planes to the over-all reactivity increases as the edge roughness factor increases. For a roughness factor of 1·4, as estimated earlier for G100, the additional contribution of reaction at basal planes would be negligible. However, if the edge roughness factor were about 25, as reported by Lang and Magnier for pyrolytic graphite[17], the basal planes would contribute about 60 per cent to the over-all reactivity, where $k_g/k = 1/25$.

Consider the edge area exposed upon oxidation down the cores of non-basal dislocations. As with the case of oxidation at crystallite boundaries, it can be shown[15] that the maximum amount of edge area produced per unit geometric basal plane area is equal to the ratio of rates, that is k_d/k, and is independent of dislocation density. If we take $k_d/k = 1/25$, as suggested by Thomas[12], the contribution of the non-basal dislocations to over-all reactivity will be equal to the contribution coming from attack at crystallite boundaries. As noted by Thomas[12], the k_d/k ratio is markedly increased if the dislocation is deliberately contaminated with an oxidation catalyst. This in turn would increase the contribution of the non-basal dislocations to over-all reactivity by increasing the edge area produced at these dislocations per unit basal plane area.

4. CONCLUSIONS

Different samples of compression annealed pyrolytic graphites have different anisotropies for their oxidation rates in directions parallel and perpendicular to the basal surface. Qualitatively, anisotropy is greater the higher the extent of crystallite alignment.

Defect models have been considered theoretically in order to estimate the contribution of reaction at defect sites in the basal plane to over-all reactivity, that is, at these defect sites plus sites at the gross edge of the pyrolytic graphite samples. It is concluded that the concentration of vacancies is insufficient for this defect to contribute significantly to over-all reactivity. On the other hand, reaction at surfaces of voids resulting from attack at non-basal dislocations and/or crystallite boundaries can make a significant contribution provided that the ratio of reactivity in the c-direction down these defects compared to reactivity in the a-direction is large. A concentration of some impurities at these defects is expected to markedly increase the contribution of reactivity at the defects to over-all reactivity since selected impurities have been shown, in the literature, to sharply increase the reaction anisotropy in the c-direction to the a-direction.

Acknowledgements—This study was supported by the Atomic Energy Commission on Contract Number AT(30–1)–1710 and a grant from Airco Speer Carbon-Graphite. Dr. Arthur Moore of the Union Carbide Corporation supplied us with the graphites used in this study.

REFERENCES

1. Rodriguez-Reinoso F., Thrower P. A. and Walker, P. L. Jr., *Carbon* **12**, 63 (1974).
2. Coffin L. F. Jr., *J. Am. Ceram. Soc.* **47**, 473 (1964).
3. Baker J. J., The Pennsylvania State University, Ph. D. Thesis (1970).
4. Horton W. S. and Ballard D. B., *Carbon* **10**, 499 (1972).
5. Evans E. L., Griffiths R. J. M. and Thomas J. M., *Science* **171**, 174 (1971).
6. Hennig G. R., *Chemistry and Physics of Carbon*, (Edited P. L. Walker, Jr.), Vol. 3. Marcel Dekker, New York, 1966, p. 180.
7. Adamson I. Y. R., Dawson I. M., Feates F. S. and Sach R. S., *Carbon* **3**, 393 (1966).
8. Feates F. S., *Trans. Faraday Soc.* **64**, 3093 (1968).
9. Feates F. S. and Robinson P. S., *Third Conference on Industrial Carbon and Graphite.* Society of Chemical Industry, London, 1971, p. 233.
10. Rodriguez-Reinoso F. and Thrower P. A., *Carbon* **12**, 269 (1974).
11. Hennig G. R., *Chemistry and Physics of Carbon*, Vol. 2. Marcel Dekker, New York, 1966, p.1.
12. Thomas J. M., *Carbon* **7**, 359 (1969).
13. Roscoe C. and Baker J. J., *J. Appl. Phys.* **40**, 1665 (1969).
14. Moore A. W., *Chemistry and Physics of Carbon*, Vol. 11. Marcel Dekker, New York, 1973, p. 69.
15. Rellick G. S., The Pennsylvania State University, M. S. Thesis (1973).
16. Roscoe C. and Thomas J. M., *Proc. Roy. Soc.* **A297**, 397 (1967).
17. Lang F. M. and Magnier P., *Chemistry and Physics of Carbon*, Vol. 3. Marcel Dekker, New York, 1966, p. 171.